

# Turbulence generation by large-scale extreme vertical drafts and the modulation of local energy dissipation in stably stratified geophysical flows

Raffaele Marino<sup>1</sup>, Fabio Feraco<sup>1,2</sup>, Leonardo Primavera<sup>2</sup>, Alain Pumir<sup>3</sup>, Annick Pouquet<sup>4,5</sup>, Duane Rosenberg<sup>6</sup>, Pablo D. Mininni<sup>7</sup>.

<sup>1</sup>*Laboratoire de Mécanique des Fluides et d'Acoustique, CNRS, École Centrale de Lyon, Université Claude Bernard Lyon 1, INSA de Lyon, F-69134 Écully, France.*

<sup>2</sup>*Dipartimento di Fisica, Università della Calabria, Italy.*

<sup>3</sup>*Laboratoire de Physique, UMR5672, École Normale Supérieure de Lyon and CNRS, 46 Allée d'Italie, F-69007, Lyon, France.*

<sup>4</sup>*Laboratory for Atmospheric and Space Physics, University of Colorado, Boulder, CO 80309, USA.*

<sup>5</sup>*National Center for Atmospheric Research, P.O. Box 3000, Boulder, CO 80307, USA.*

<sup>6</sup>*288 Harper St. Louisville, CO 80027 USA.*

<sup>7</sup>*Departamento de Física, Facultad de Ciencias Exactas y Naturales, Universidad de Buenos Aires, and IFIBA, CONICET, Buenos Aires 1428, Argentina.*

We observe the emergence of strong vertical drafts in direct numerical simulations of the Boussinesq equations in a range of parameters of geophysical interest. These structures, which appear intermittently in space and time, generate turbulence and enhance kinetic and potential energy dissipation, providing an explanation for the observed variability of the local energy dissipation in the ocean and the modulation of its probability distribution function. We show how, due to the extreme drafts, in runs with Froude numbers observable in oceans, roughly 10% of the domain flow can account for up to 50% of the total volume dissipation, consistently with recent estimates based on oceanic models.

The combination of turbulent eddies and waves, due to stratification and rotation, leads to the formation of surprising features in geophysical flows, from oval structures and jets on Jupiter [1], to hurricanes and tornadoes in our atmosphere [2], or strong currents and dual energy cascades in the ocean [3–8]. The interplay between such structures is not fully understood, in particular their dependence on control parameters such as the Reynolds and Froude numbers [9–11] (see below for definitions). But it is known that extreme events associated with these structures can play an important role. For example, high vertical drafts are observed in the planetary boundary layer [12–14], as well as strong winds in the lower troposphere [15, 16]. In the ocean, vast regions of rather constant energy dissipation  $\varepsilon_0$  are observed together with local patches of turbulence dissipating  $10^2 - 10^4$  times  $\varepsilon_0$ , as in the vicinity of the Hawaiian ridge [4] or of the Puerto-Rico trench [17], with large values of the vertical velocity [18, 19]. In frontal structures, gradients of tracers such as pollutants are characterized by very large fluctuations, with a kurtosis (the normalized fourth moment of the distribution) reaching values of several hundreds [20]: all these extreme events are characterized by non-Gaussian statistics.

Recent numerical work based on the Boussinesq equa-

tions has confirmed that the vertical component of the velocity field ( $w$ ) exhibits a large-scale intermittent behavior, in both space and time, for values of parameters of geophysical interest [21]. In particular, direct numerical simulations (DNSs) of stably stratified turbulent flows were found to systematically develop powerful vertical drafts that make the statistics of  $w$  strongly non-Gaussian in the energy-containing eddies. This is interpreted as a result of the interplay between gravity waves and turbulent motions, and it occurs in a resonant regime of the governing parameters where vertical velocities are enhanced much faster than in the analogous homogeneous isotropic turbulence (HIT) case [21, 22]. It can also be understood as a result of complex phase-space dynamics in a reduced model for the velocity and temperature gradients [23]. The present study establishes that extreme drafts emerge in a recurrent manner in stratified flows, producing localized turbulence, and ultimately bursts of dissipation at small-scale.

**Simulations and parameters:** We performed a series of DNSs in a triply-periodic domain of side  $2\pi L_0$  with  $512^3$  grid points for up to  $t \approx 500\tau_{NL}$  ( $\tau_{NL} = L/U$  being the turnover time,  $U$  and  $L$  the flow characteristic velocity and integral scale respectively in units of a simulation unit length  $L_0$  and a unit velocity  $U_0$  with

Run	P1	P2	P3	P4	P5	P6	P7	P8	P9
Re [ $\times 10^3$ ]	2.4	2.6	3.6	3.8	3.8	3.8	3.8	1.2	0.8
Fr [ $\times 10^{-1}$ ]	$\infty$	2.8	1.1	0.81	0.76	0.3	0.26	0.76	0.71
$R_B$	$\infty$	206	43.8	24.8	22.1	3.4	2.6	6.8	4.2
$\nu[\times 10^{-3}L_0U_0]$	1.5	1	1	1	1	1	1	3	4
$N [U_0/L_0]$	0	1.5	5	7.37	8	20	23.5	7.37	7.37
$t_{tot}/\tau_{NL}$	30	55	103	452	406	91	62	526	422

TABLE I. Parameters of the runs, with Re, Fr, and  $R_B$  respectively the Reynolds, Froude, and buoyancy Reynolds numbers, and  $\nu$ ,  $N$ , and  $t_{tot}/\tau_{NL}$  the kinematic viscosity, the Brunt-Väisälä frequency, and the temporal extension of the runs in units of the turnover time.

$T_0 = L_0/U_0$ ). Some of these flows were analyzed in [21] over a limited time span (up to  $\approx 25\tau_{NL}$ ), while other simulations are new. It was shown that the kurtosis of  $w$  could reach high values in a narrow regime of parameters around a Froude number  $Fr = U/(LN) \approx 0.08$ , with  $N = [-(g/\rho_0)\partial_z\bar{\rho}]^{1/2}$  the Brunt-Väisälä frequency,  $\rho_0$  the mean density and  $\bar{\rho}$  the background linear density profile. Simulation parameters are listed in Table I. Runs P3 to P5, with  $5 \leq NT_0 \leq 8$ , correspond to the resonant regime mentioned above. In all the simulations with  $N \neq 0$ ,  $NT_0$  varies from 1.5 to 23.5. As a reference, a typical velocity in the ocean of  $U_0 = 0.1\text{ms}^{-1}$ , and a unit length of 1 km (thus for a domain of  $\approx 6.3$  km), results in  $N \approx 2 \times 10^{-3} \text{ s}^{-1}$  (for run P7) to  $N \approx 10^{-4} \text{ s}^{-1}$  (for P2). These values are reasonable for oceanic scales and situations in which the hydrostatic approximation breaks down [24].

The Boussinesq equations for the velocity  $\mathbf{u}$  and the buoyancy  $\theta = g\rho'/(N\rho_0)$  (where  $\rho'(\mathbf{x})$  are the density fluctuations around the stable linear background) are [25]:

$$\partial_t \mathbf{u} + (\mathbf{u} \cdot \nabla) \mathbf{u}, = -\nabla p - N\theta \hat{z} + \mathbf{F}_u + \nu \nabla^2 \mathbf{u} \quad (1)$$

$$\partial_t \theta + \mathbf{u} \cdot \nabla \theta = Nw + \kappa \nabla^2 \theta; \quad (2)$$

$\kappa$  is the thermal diffusivity and  $\nu$  the kinematic viscosity, with  $\kappa = \nu$  for all runs. Both values, in units of  $L_0U_0$ , are not realistic for geophysical flows and come as a result of computational constraints, and should be considered as effective transport coefficients.

The Reynolds and buoyancy Reynolds numbers are  $Re = UL/\nu$ ,  $R_B = ReFr^2$ .  $R_B$  is a measure of the relative strength of the buoyancy to the dissipation, identifying three regimes: one controlled by gravity waves ( $R_B \leq 10$ ), a transitional regime, and another dominated by turbulence ( $R_B \geq 10^2$ ) [10, 21]. Fr, Re, and  $R_B$  are computed for each run close to the peak of the dissipation. A HIT run is also performed. The flows evolve under the action of a random forcing  $\mathbf{F}_u$ , with constant amplitude, delta-correlated in time, isotropic in Fourier space, and centered on a spherical shell of wavenumbers  $2 \leq k_f \leq 3$ . Simulations used the GHOST code (Geophysical High Order Suite for Turbulence), a highly par-

allelized pseudo-spectral framework that hosts a variety of solvers [26–28] to study anisotropic classic and quantum fluids, as well as plasmas.

**Generation of turbulence by extreme vertical drafts:** The presence of strong drafts is investigated through the analysis of the temporal evolution of the kurtosis,  $K_w = \langle (w - \langle w \rangle)^4 \rangle / \langle (w - \langle w \rangle)^2 \rangle^2$ , computed as a function of time from the simulations. We recall that the kurtosis of a Gaussian distribution is  $K = 3$ , so values of  $K_w > 3$  are indicative of the presence of extreme events in  $w$ . Figure 1 displays  $K_w$  vs.  $t/\tau_{NL}$  for runs P4, P5, P8, and P9. The values of the Froude number for these runs are close to  $Fr \approx 0.08$ , for which  $K_w$  was found to be maximum from calculations at  $Re \approx 3800$  in [21]. Such values of Fr are compatible with estimates in some regions of the ocean [29]. To characterize how these extreme drafts affect the flow energetics, we accumulate the statistics for several hundreds  $\tau_{NL}$  (see Tab. I). Together with the investigation of this global quantity, our study will later consider statistical tools which are local, either in Fourier or in physical space. Starting from the

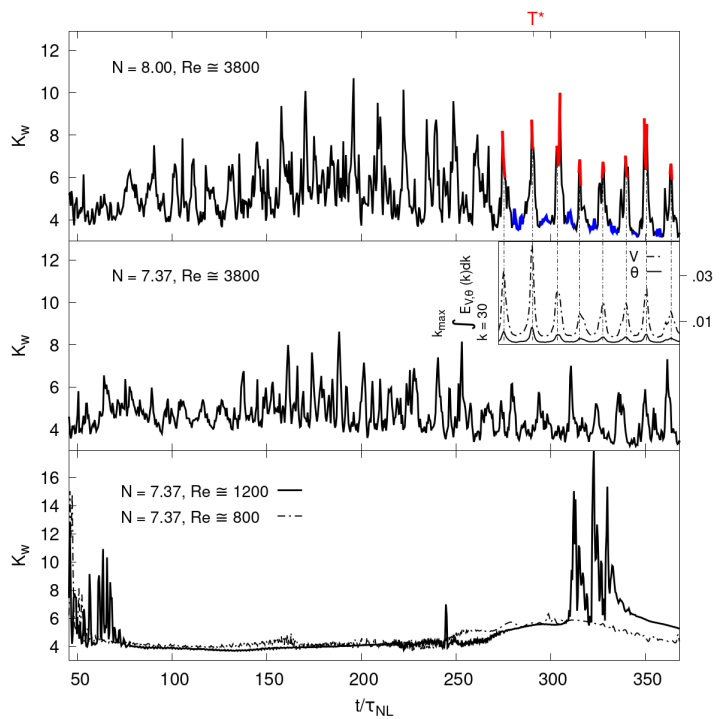


FIG. 1. Kurtosis  $K_w$  of the vertical velocity  $w$  as a function of time, in units of the turn-over time  $\tau_{NL}$ , for runs P5 (upper panel), P4 (middle), as well as (lower panel) P8 (solid line) and P9 (dashed line). Red and blue identify respectively the portions of the signal across relative maxima and minima used to compute the spectra in Fig.2.  $T^*$  is the reference time used in Figs. 3 & 4. The inset in the middle panel shows the small-scale energy at late times for run P5.

top panel of Fig. 1 we observe that, for  $N = 8.0U_0/L_0$ ,

the flow is characterized by strong spikes of the kurtosis reaching values as high as  $K_w \approx 11$ , and separated by short time intervals with values of  $K_w$  close to the Gaussian reference. The temporal analysis of the high-order spatial statistics allows us to conclude that in the presence of large-scale intermittent drafts not only the flow is non-homogeneous due to the irregular emergence of these structures, but furthermore, global properties of the flow exhibit wide fluctuations. A similar situation has been observed in other flows, such as turbulent homogeneous shear flows [30, 31]. The fluctuations of  $K_w$  are smaller for  $N = 7.37U_0/L_0$  (middle panel), which is still close to  $Fr \approx 0.08$  and also appears to show fluctuations of large scales quantities. Keeping  $N = 7.37U_0/L_0$  but lowering the Reynolds number to  $Re \approx 1200$  changes drastically the dependence of  $K_w$  on  $t/\tau_{NL}$ : it becomes a smooth signal interrupted by sporadic bursts. The signal is almost completely smooth and stationary for  $Re \approx 800$  (Fig. 1, bottom). Since  $Fr$  for the three runs is roughly the same, this transition appears therefore led by  $R_B$ .

To investigate how strong vertical drafts affect the generation of turbulence, we performed a systematic study of the isotropic kinetic and potential energy spectra,  $E_V(k)$  and  $E_\theta(k)$ . The results indicate a substantial enhancement of the power spectral density (PSD) in the small scales when  $K_w$  is maximal. This can be clearly inferred from the spectra computed at local maxima and minima of the kurtosis, as shown in Fig. 2 for run P5 (corresponding to times highlighted in red and blue in Fig. 1). The small-scale PSD of  $E_V(k)$  and  $E_\theta(k)$  computed at the local maxima can be up to four orders of magnitude larger than the corresponding PSD for neighboring local minima. This indicates that vertical drafts excite small-scale turbulent structures, developing in patches within the flow, and powerful enough to modify the spectral distribution of the energy, plausibly with a  $k^{-5/3}$  dependence over an inertial range of scales at the times when  $K_w$  peaks (see insets in Fig. 2). Conversely, the energy spectra computed at the local minima are much lower for  $k > 10$ , and in fact steeper, plausibly with a  $k^{-2}$  scaling at intermediate scales. The integral of  $E_V(k)$  and  $E_\theta(k)$  for  $k > 30$ , proxies respectively of the small-scale kinetic and potential energy, are shown in the inset of Fig. 1. Their correlation with the local maxima and minima of  $K_w$  confirms that enhancements of the small-scale PSD are modulated by the presence of extreme vertical drafts.

**Modulation of kinetic energy dissipation:** A systematic study of the statistics of the kinetic energy dissipation rate  $\varepsilon_V = \nu(\partial u_i/\partial x_j)(\partial u_i/\partial x_j)$  reveals that the extreme vertical drafts strongly feedback on  $\varepsilon_V$ , and play a major role in the way kinetic energy is dissipated in stratified turbulence. Figure 3 shows the instantaneous vertical profile of the kurtosis  $K_w(z, T^*)$  (i.e., averaged over horizontal planes of constant height) in run P5, at

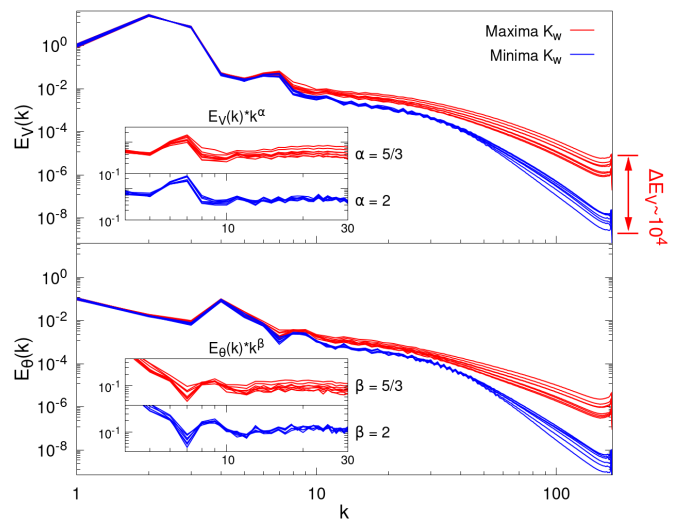


FIG. 2. Kinetic (top) and potential (bottom) energy spectra computed for run P5 at the relative maxima (red) and minima (blue) of  $K_w$  (see Fig. 1). Insets show compensated spectra.

time  $T^* \approx 290\tau_{NL}$ , when  $K_w(T^*)$  is at a maximum (see Fig. 1). The figure also shows the vertical profile of the dissipation rate  $\hat{\varepsilon}_V(z, T^*)$ , normalized by its value in the entire volume (so that  $\int_0^{2\pi} \hat{\varepsilon}_V(z, T^*) dz = 1$ , again averaged over horizontal planes), and probability density functions (PDFs) of  $\hat{\varepsilon}_V$  in regions at different heights. A comparison between the profiles of  $K_w$  and  $\hat{\varepsilon}_V$  reveals some correlation between their peaks (Fig. 3, right). The PDFs for regions with strong (I, II), moderate (IV) and weak (III, V) local dissipation show that the statistical distribution of the kinetic energy dissipation is modulated by the presence of extreme vertical drafts (Fig. 3, left). Indeed  $P[\log(\varepsilon_V)]$  is similar between regions with comparable values of  $K_w$ .

Figure 4 gives vertical profiles of the by-plane kurtosis  $K_w(z, t)$  and of the normalized kinetic energy dissipation  $\hat{\varepsilon}_V(z, t)$ , as a function of time around  $T^*$  for run P5. Note how large peaks of dissipation occur in the flow immediately after developing strong vertical drafts, detected through the height of the kurtosis. Indeed, the point-wise values of the quantities rendered in Fig.4 are maximally correlated for a time delay of  $\hat{\phi} \approx \tau_{NL}/3$ , as it results from the analysis of the distance correlation coefficient. The latter measures both linear and nonlinear correlation between  $X = K_w(z, t)$  and  $Y = \hat{\varepsilon}_V(z, t + \hat{\phi})$ , for different temporal shifts  $\hat{\phi}$  (inset in the bottom panel of Fig.4):

$$dCor_{XY} = \frac{\mu_{XY}}{(\mu_{XX}^2 \mu_{YY}^2)^{1/4}} \quad (3)$$

where  $\mu_{XY}$ ,  $\mu_{XX}$  and  $\mu_{YY}$  are defined as in [32, 33]. It is worth noticing that the overall correlation is always rather high,  $\sim 46\%$ , even for  $\hat{\phi} = 0$ . Finally, the joint PDF of  $K_w(z, t)$  and of  $\hat{\varepsilon}_V(z, t)$  for all times and heights

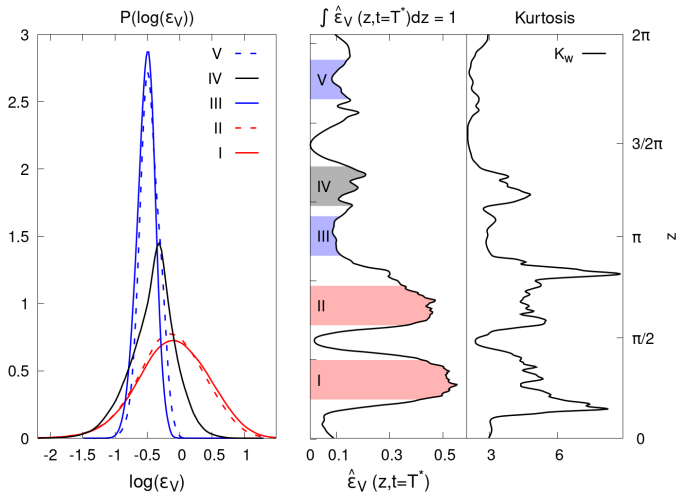


FIG. 3. Left: PDFs of the kinetic energy dissipation computed in the regions indicated by the shaded areas in the mid panel, for run P5. Middle: profile of the normalized kinetic energy dissipation  $\hat{\varepsilon}_V(z, t)$  in individual horizontal planes, at fixed time  $T^*$  and as a function of  $z$ . Right: vertical profile of the by-plane kurtosis  $K_w(z, t)$ .

available for P5 is shown in the bottom panel of Fig. 4, together with the conditional average of the dissipation in bins of the kurtosis,  $\langle \hat{\varepsilon}_V(z, t) | K_w(z, t) \rangle$  (red line). Note that, locally in space and time, larger values of  $K_w$  correspond to larger dissipation rates up to  $K_w \approx 6$  while for  $K_w > 6$ ,  $\hat{\varepsilon}_V(z, t)$  saturates, these high  $K_w$  regions being very efficient at dissipating kinetic energy. The good correlation resulting from the above statistics, together with the evidence that local maxima of  $\hat{\varepsilon}_V(z, t)$  are anticipated by peaks in  $K_w(z, t)$ , prove quantitatively the causation between the emergence of vertical drafts and the enhancement of the dissipation. Similar results are obtained for other simulations. Overall, these results indicate that the local occurrence of extreme drafts determines the local properties and statistics of strong dissipative events.

**Enhanced local dissipation efficiency:** The efficiency of the local energy dissipation can be further characterized by computing the minimal domain volume needed to achieve a given percentage of the total energy dissipation at a given time. We evaluate the local kinetic and potential energy dissipation efficiency, respectively  $V_{\varepsilon_V}$  and  $V_{\varepsilon_\theta}$  (with  $\varepsilon_\theta = \kappa |\nabla \theta|^2$ ), by classifying the temporal outputs of each run in terms of their global kurtosis  $K_w$ , and then computing the minimal volume needed to achieve the 50% level of the global energy dissipation.

The outcome of this analysis is shown in Figure 5 for the runs with  $2400 \leq Re \leq 3800$ , in order to avoid any Reynolds dependence of  $V_{\varepsilon_V}$  and  $V_{\varepsilon_\theta}$ . First, we note that the HIT case has one of the highest kinetic energy dissipation efficiencies: only  $\approx 15\%$  of the most dissipative regions within the volume are in fact needed to achieve 50% of the global dissipation (Fig. 5, top). Strongly

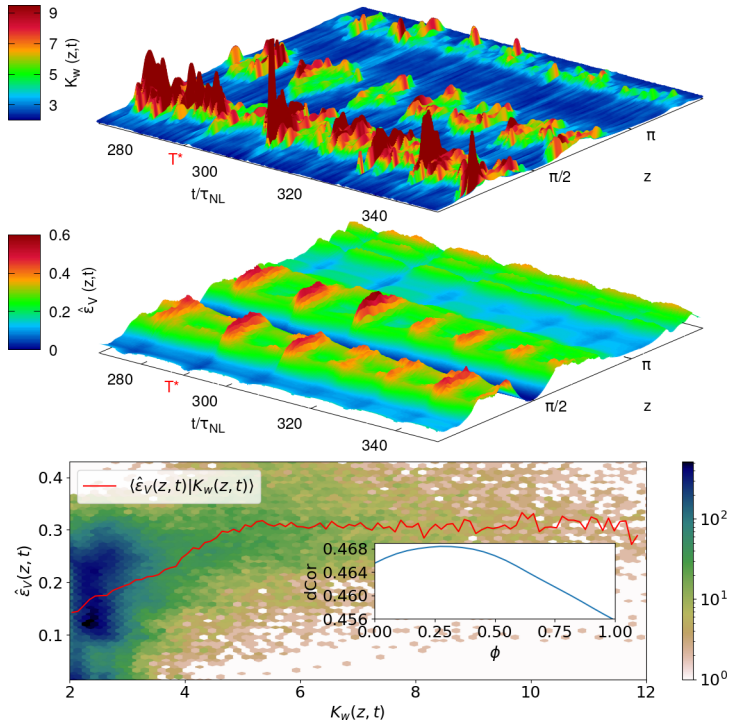


FIG. 4. Temporal evolution in units of  $\tau_{NL}$  for run P5 of (top) the vertical profile of the by-plane kurtosis  $K_w(z, t)$ , and (mid-top) the normalized kinetic energy dissipated in horizontal planes  $\hat{\varepsilon}_V(z, t)$ , around  $T^*$ . The bottom panel gives the joint PDF of  $K_w(z, t)$  and  $\hat{\varepsilon}_V(z, t)$  for all P5 data, the solid red line indicating averages of  $\hat{\varepsilon}_V$  conditioned on  $K_w$ . Inset: evolution of the distance correlation coefficient  $dCor$  between  $K_w(z, t)$  and  $\hat{\varepsilon}_V(z, t + \phi)$ , as a function of a temporal lag  $\phi$  between the two signals

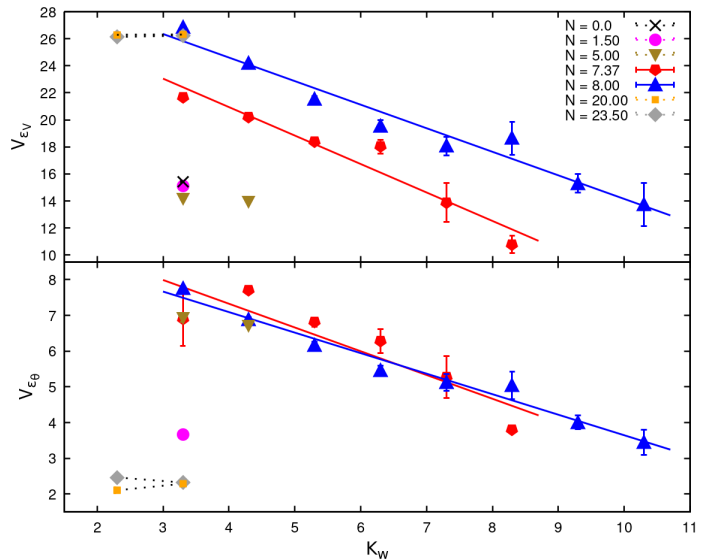


FIG. 5. Kinetic and potential energy dissipation efficiency as a function of  $K_w$  for high-Re runs P1–P7 measured in terms of the minimal domain volumes  $V_{\varepsilon_V}$  and  $V_{\varepsilon_\theta}$  needed to achieve 50% of respectively the total kinetic and potential energy dissipation.

stratified flows are unable to achieve a similar  $V_{\varepsilon_V}$  except when they develop extreme drafts, powerful enough that  $K_w \gtrsim 7$ , attainable in our study only for Froude numbers within the resonant regime delineated in [21] (runs P5 and P4), a regime compatible with values found in some regions of the ocean and the atmosphere. Indeed,  $V_{\varepsilon_V}$  for these two runs can be respectively as low as  $\approx 14\%$  and  $\approx 11\%$ , smaller in fact than for the HIT case. Thus, not only do the large-scale vertical drafts generate small-scale turbulence, but they are also responsible for the local and efficient enhancement of the kinetic energy dissipation  $\varepsilon_V$ . The drafts are then needed, when stratification is strong ( $Fr \lesssim 0.1$ ), for the energy to be locally dissipated as efficiently as in the HIT case at equivalent Reynolds numbers.

Indeed, without drafts, dissipation efficiency is significantly smaller. The most stratified runs in our study (runs P7 and P8) are unable to develop significant drafts, and they are both characterized by an efficiency  $V_{\varepsilon_V} \approx 26\%$ , more than twice that of the most dissipative cases of runs P4 and P5. On the opposite limit, when stratification is weak, as for runs P2 and P3,  $V_{\varepsilon_V}$  approaches the value of the HIT case (in fact from below) even though  $K_w \approx 3$ . The local potential energy dissipation efficiency  $V_{\varepsilon_\theta}$  exhibits a behaviour similar to that of  $V_{\varepsilon_V}$  (Fig. 5, bottom) except for the most stratified runs P7 and P8, that appear to be the most dissipative, although characterized by low kurtosis  $K_w$ . Moreover, values of  $V_{\varepsilon_\theta}$  are smaller than those of  $V_{\varepsilon_V}$ , suggesting that stratified flows are more efficient in dissipating potential energy than kinetic energy. This could be related to the well-known stronger small-scale intermittency of (passive) scalars as they easily form frontal structures [34, 35].

**Conclusions:** We show that the generation of large-scale intermittent vertical drafts in stratified turbulence [21] can lead to recurrent strong modulations of the flow over durations of  $\gtrsim 400 t/\tau_{NL}$ . These extreme events produce, through instabilities, strong localized energy dissipation  $\varepsilon_V$  and modulate the overall distribution  $P(\varepsilon_V)$ , whose shape depends on the region of the flow considered. This result sheds light on the variability of the kinetic energy dissipation observed in the ocean, as well as on the link between intermittency and dissipation [36]. Indeed, it provides a mechanism for the modulation of the PDF of  $\varepsilon_V$ , as recently reported by Pearson et al. in global model simulations of the ocean [37], where macroscopic features of the distributions (such as the mean and standard deviation) depend on the ocean depth and the sub-domains considered. The presence of vertical drafts is also needed for stably stratified turbulence to achieve a localized dissipation efficiency comparable to that of homogeneous isotropic turbulence. In particular, we showed that, at the peak in  $Fr$  of the resonant regime identified in [21], roughly 10% of the domain volume ( $V_{\varepsilon_V}$ ) is sufficient to account for 50% of the

total dissipation which, considering the simplified setup of our DNS with respect to the complexity of oceanic flows, is compatible with the results presented in [37] modeling the global ocean. Thus, the way energy is dissipated in geophysical flows is an important open problem; our study indicates that in a certain region of parameter space vertical drafts and the associated steepening of gravity waves can lead to enhanced local-in-time-and-space dissipation, ultimately leading to an inadequacy of the description of the system in terms of weakly interacting waves, even when the global Froude number is small.

R. Marino acknowledges support from the project “EVENTFUL” (ANR-20-CE30-0011), funded by the French “Agence Nationale de la Recherche” - ANR through the program AAPG-2020. A. Pouquet is thankful to LASP and in particular to Bob Ergun.

- 
- [1] P. S. Marcus, *Annu. Rev. Astron. Astrophys.* **31**, 523 (1993).
  - [2] K. Emanuel, *Nature* **436**, 686 (2005).
  - [3] R. Scott and F. Wang, *J. Phys. Oceano.* **35**, 1650 (2005).
  - [4] J. M. Klymak, R. Pinkel, and L. Rainville, *J. Phys. Oceano.* **38**, 380 (2008).
  - [5] P. Klein, B. L. Hua, G. Lapeyre, X. Capet, S. L. Gentil, and H. Sasaki, *J. Phys. Oceano.* **38**, 1748 (2008).
  - [6] R. Marino, A. Pouquet, and D. Rosenberg, *Phys. Rev. Lett.* **114**, 114504 (2015).
  - [7] J. Xie and O. Bühler, *Journal of Fluid Mechanics* **872**, 752 (2019).
  - [8] J. Xie and O. Bühler, *Journal of Fluid Mechanics* **851**, 672 (2018).
  - [9] R. Marino, D. Rosenberg, C. Herbert, and A. Pouquet, *EuroPhys. Lett.* **112**, 49001 (2015).
  - [10] A. Pouquet, D. Rosenberg, R. Marino, and C. Herbert, *J. Fluid Mech.* **844**, 519 (2018).
  - [11] H. Wang and O. Bühler, *Journal of Fluid Mechanics* **882**, A16 (2020).
  - [12] J. L. Chau, R. Marino, F. Feraco, C. Urco, M. Juan, G. Baumgarten, F.-J. Luebken, W. K. Hocking, C. Schult, T. Renkowitz, and R. Latteck, *Earth and Space Science Open Archive* 20 (2021).
  - [13] D. H. Lenschow, M. Lothon, S. D. Mayor, P. P. Sullivan, and G. Canut, *Bound. Lay. Met.* **143**, 107 (2012).
  - [14] L. Mahrt, *J. Atmos. Sci.* **46**, 79 (1989).
  - [15] L. Mahrt and N. Gamage, *J. Atmos. Sci.* **44**, 1106 (1987).
  - [16] H. L. Liu, *Geophys. Res. Lett.* **34**, L08815 (2007).
  - [17] H. van Haren and L. Gostiaux, *J. Mar. Res.* **74**, 161 (2016).
  - [18] E. D’Asaro, R.-C. Lien, and F. Henyey, *J. Phys. Oceanogr.* **37** (2007).
  - [19] X. Capet, J. McWilliams, M. Molemaker, and A. Shchepetkin, *J. Phys. Oceanogr.* **38** (2008).
  - [20] J. Klymak, W. Crawford, M. H. Alford, J. A. MacKinnon, and R. Pinkel, *J. Geophys. Res.* **120**, 2287 (2015).
  - [21] F. Feraco, R. Marino, A. Pumir, L. Primavera, P. Mininni, A. Pouquet, and D. Rosenberg, *Eur. Phys. Lett.* **123**, 44002 (2018).

- [22] C. Rorai, P. Mininni, and A. Pouquet, *Phys. Rev. E* **89**, 043002 (2014).
- [23] N. Sujovolsky and P. Mininni, *Phys. Rev. F* **5**, 064802 (2020).
- [24] G.K. Vallis, *Atmospheric and Oceanic Fluid Dynamics*, Cambridge Univ. Press (2006).
- [25] P.A. Davidson Cambridge Univ. Press (2013).
- [26] P. Mininni, D. Rosenberg, R. Reddy, and A. Pouquet, *Parallel Computing* **37**, 316 (2011).
- [27] M. Fontana, O. P. Bruno, P. D. Mininni, and P. Dmitruk, *Comp. Phys. Comm.* **256**, 107482 (2020).
- [28] Duane Rosenberg, Pablo D. Mininni, Raghu Reddy, and Annick Pouquet, *Atmosphere* **11**, 178 (2020).
- [29] M. Nikurashin, *J. Phys. Oceano* **40**, 1055-1074 (2010).
- [30] A. Pumir, *Phys. Fluids* **8**, 3112 (1996).
- [31] A. Sekimoto, S. Dong, and J. Jiménez, *Phys. Fluids* **28**, 035101 (2016).
- [32] G.J. Székely, M.L. Rizzo, and N.K. Bakirov, *The Annals of Statistics* **35**, 2769-2794 (2007).
- [33] D. Edelmann, K. Fokianos, and M. Pitsillou, *International Statistical Review* **87**, 237-262 (2019).
- [34] A. Pumir, *Phys. Fluids* **6**, 2118 (1994).
- [35] N.E. Sujovolsky, P.D. Mininni, and A. Pouquet, *Physics of Fluids* **30**, 086601 (2018).
- [36] J. Isern-Fontanet and A. Turiel, <https://arxiv.org/pdf/2012.01385.pdf>.
- [37] B. Pearson and B. Fox-Kemper, *Phys. Rev. Lett.* **120**, 094501 (2018).